CrossMark

Preparation and property assessment of neat lignocellulose nanofibrils (LCNF) and their composite films

Thomas Horseman · Mehdi Tajvidi · Cherif I. K. Diop · Douglas J. Gardner

Abstract Lignocellulose nanofibrils (LCNF) were produced from thermo-mechanical pulp (TMP) using a micro-grinder and were characterized with respect to fiber diameter and thermal stability. The initial water content in the TMP affected the defibrillation process and longer grinding time was necessary for the air-dried TMP, resulting in LCNF with higher fibril diameter. As compared to the reference cellulose nanofibrils (CNF) produced through a refining process, LCNF was less thermally stable and started to degrade at a temperature that was 30 °C lower than that of CNF. LCNF obtained from the never-dried TMP was combined with various additives (10 wt%) to produce composite films. The neat LCNF and composite films did not reach the mechanical properties of the neat CNF film that was evaluated as reference. However, the addition of poly(vinyl alcohol) (PVA) at 10 wt% on a dry basis did cause a 46 and 25% increase in tensile strength and elastic modulus, respectively. Other additives including cellulose nanocrystals, bentonite and CNF were also found to increase to some extent the Young's modulus and ductility of the LCNF composite films whereas the addition of talc did not improve the film performance. Water absorption of neat LCNF films was lower than the reference CNF and was negatively affected by the addition of PVA.

Keywords Mechanical fibrillation · Lignocellulose nanofibrils · Composite films · Mechanical properties · Thermal stability

T. Horseman
Rose-Hulman Institute of Technology, Terre Haute, IN 47803, USA

M. Tajvidi (✉)
School of Forest Resources and Advanced Structures and Composites Center, University of Maine, 117 Nutting Hall, Orono, ME 04469, USA
e-mail: mehdi.tajvidi@maine.edu

C. I. K. Diop
School of Forest Resources, University of Maine, Orono, ME 04469, USA

D. J. Gardner
School of Forest Resources and Advanced Structures and Composites Center, University of Maine, Orono, ME 04469, USA

Introduction

The United States historically and still today leads the world economy in consumption and production of forest products. As the demand for forest-based products shifts with the development of other countries and strengthening global environmental awareness, a new and promising nanomaterial made from cellulose has emerged (Wear et al. 2015). Cellulose is the most abundant natural biopolymer on Earth and is a clean and renewable material. Nanocellulose technology is gaining popularity as research shows it is a viable substitute to petroleum in engineered materials

such as packaging, adhesives, and films. Extensive studies on cellulose nanofibrils' (CNF) production and application have been conducted due to their favorable properties such as biodegradability, low density, large aspect ratio, high modulus, and hydrophilicity (Bharimalla et al. 2015; Khalil et al. 2014).

A major factor limiting the application of CNF in industry is the energy cost associated with overcoming the bonding mechanisms that holds the fibrils of cellulose together. There are two main kinds of pulps in the pulp and paper industry which can serve as precursors to CNF, chemical, and mechanical pulps. Mechanical pulping is a process in which wood is subjected to mechanical shearing forces that separate the wood fibers (Osong 2014). These pulps are typically pre-treated with chemicals or enzymes to lower the energy consumption in the grinding process and to improve fibrillation (Bharimalla et al. 2015; Khalil et al. 2014; Osong 2014). The actual production of CNF consists of intensive mechanical treatments of the pulp, the most common of which is refining and high-pressure homogenization. Studies have shown that using micro-grinding (without chemical pretreatment) instead of high-pressure homogenization reduces the energy input costs and results in films with superior physical, optical, and water interaction properties (Spence et al. 2011).

Chemical or enzymatic pretreatment of pulps is used to remove the lignin and hemicelluloses that are associated with tree material (Khalil et al. 2014; Osong et al. 2013). This pretreatment, however, takes away from the "green" footprint of nanocellulose as chemical waste is produced in the bleaching process. Starting with thermo-mechanical pulp (TMP) a micro-grinder can be used to produce lignocellulose nanofibrils (LCNF) requiring less energy input and no chemical/enzymatic pretreatments. The size of the fibrils can be controlled by adjusting the grinder disk spacing and the number of repeated passes (Kojima et al. 2014).

The potential energy saving and improvement in physical properties has driven researchers across the world to compare LCNF to CNF in a variety of production techniques and applications. Homogenization can easily be scaled up for industrial applications and can also operate continuously (Spence et al. 2011). For this reason, studies have focused on the production of LCNF using a homogenizer where the pulp is passed through a valve and an impact ring. The high shear and impact forces caused by rapid pressure drops in the homogenizer are able to separate the fibrils of cellulose. A downside to this production technique is that the fibrils tend to clog the valve of the homogenizer. For this reason studies have gone to show that it is possible to produce LCNF from TMP with a homogenizer, that higher concentrations of unbleached TMP slurries are able to pass through the homogenizer without clogging as compared to bleached kraft pulp, and the weighted length distribution of fibrils plays a key role in the clogging of the homogenizer valve (Osong et al. 2013). The large energy consumption and potential for clogging have led researchers to compare different production techniques like micro-grinding and micro-fluidization. Micro-grinding was found to be a viable alternative since the pretreatment step needed when using high pressure-homogenization and micro-fluidization is not necessary. In addition the specific energy consumed during micro-grinding is among the lowest (Spence et al. 2011).

In this study TMP from mixed softwood was ground in a micro-grinder to produce LCNF. The LCNF product was then compared with a reference CNF produced from bleached pulp by refining. By controlling the disk spacing and length of time that the slurry is recycled through the micro-grinder, the fibril size can be controlled. The fibrils were then characterized with respect to average fibril diameter and thermal stability. It was expected that cellulose nanofibrils containing lignin would be less thermally stable than bleached CNF used as reference. Never-dried TMP and air-dried TMP were processed to produce different types of LCNF. The LCNF sample having a narrower average particle diameter distribution and a higher percent of fines in its slurry was used in the production of the neat LCNF and the LCNF composite films, using a solution casting method. The thermal stability of LCNF was evaluated and compared to the reference CNF.

The mechanical and physical properties of different films were determined. Tensile test was performed to determine the Young's modulus, tensile strength, and strain at failure. The microstructures of the films' surfaces and cross-sections were evaluated via SEM. The FT-IR spectra of the different films were compared and the changes in the water absorption of the neat and composite films were determined.

Materials and methods

Production of LCNF

Mixed softwood chips from Maine forests were pulverized into a pulp with a Bauer Disc Mill (Andritz-Sprout, Muncy, PA) at 2200 rpm under atmospheric pressure. The consistency of the chips was maintained at 35% by continuously injecting water in the refining chamber. Three stages of refining were performed, and the gap between the stationary and rotating discs was decreased after each stage. The resulting TMP was dewatered by spinning to a final moisture content of 74% and cold stored at 4 °C until further analysis. A fraction of TMP from the same batch was air dried at ambient temperature for a week to reach a moisture content of 12%.

The never-dried and air dried TMP were used to produce LCNF. The different TMPs were diluted to a 3 wt% consistency and fed into a super masscolloider (Masuko Sangyo, Kawaguchi-city, Japan) running at 2200 rpm. The space between discs was set at -15 μm once the zero gap was determined. The fiber-rich slurry was recirculated in the system allowing multiple grinding stages. An aliquot of the LCNF solution sample was withdrawn every 30 min to analyze the percent fines (fines %) in the fiber rich-slurry using a MorFi (TechPap, Saint-Martin-d'Hères, France) system. For the never dried TMP, processing time was fixed at 1.5 h and the produced suspensions were named LCNF M2. A longer grinding time of 3 h was applied to the air-dried TMP and the resulting product was named LCNF M3. The different LCNF slurries at 3% average consistency, were cold stored until further application. The reference CNF was obtained from the University of Maine Process Development Center at 3.1% solids and contained on average 95% of fines.

Characterization of LCNF

The fine percentages were calculated for LCNF M2 (milled 1.5 h produced from never-dried TMP) and LCNF M3 (milled 3 h and produced from dried TMP) as explained above. Thermal stability tests were conducted on the TMP, LCNF M2, and the reference CNF as well as on INDULIN AT kraft pine lignin using a TA Q500 thermogravimetric analyzer (TA Instruments, New Castle, DE). The materials were subjected to a heat ramp of 10.0 °C/min up to 600 °C in N$_2$ atmosphere. An isothermal thermogravimetric test was also performed with ramping initially set at 100.0 °C/min to a temperature of 280 °C, at which the furnace was held isothermal for 30 min.

The extent of fibrillation and fiber diameters across the two LCNF M2 and LCNF M3 batches were observed through light microscopy using an optical microscope model T490B-30 W-DK (Amscope Company, USA) and atomic force microscopy (AFM) (ezAFM Nanomagnetics Instruments, UK). ImageJ, an image processing and analysis software provided by the National Institute of Health was used to measure average diameters of the CNF and LCNF fibrils. An average of 100 measurements was made for each sample in order to determine their average fibril diameter and diameter distribution.

Film preparation and characterization

LCNF M2 produced after 1.5 h of milling from never-dried TMP was used in the production of films. It was diluted in distilled water in order to form a 1% solution that was used as the film matrix. Casting evaporation method was used to prepare the neat and composite films. Reference films were made using the reference CNF at 1% consistency. LCNF was subsequently blended with cellulose nanocrystals (CNC) (received at 11.8% solids; University of Maine Process Development Center), PVA (Sigma-Aldrich; M.W. 85,000–124,000; degree of hydrolysis ≥99%; product code 1001840877), talc powder (10 μm; Sigma-Aldrich; product code 1001877676), and bentonite (specific gravity 2.6; Nanocor PGN) in order to produce composite films. A 5% PVA solution was first prepared by dissolving the PVA granules in water at 90 °C for 2 h under magnetic stirring. In all cases, except for the neat films, the compositions of the films were 90 wt% LCNF and 10 wt% additives. The mixtures of LCNF and additives were manually homogenized using a glass rod, then sonicated for 90 s with a VWR Scientific Branson Sonifier 450 at 80% power level. Thirty grams of each formulation was poured into a petri dish and allowed to dry at room temperature for 48 h.

The thickness of the dried films were measured in different areas of the material, using a Marathon Electronic Digital Micrometer. The average thickness of the films was 0.060 mm ± 0.005 mm. Tensile testing measurements were performed on 3 × 30 mm

film strips using a DMA Q800 V21.1 Build 51 (TA Instruments, New Castle, DE). Five samples of each film were subjected at a force ramp of 4.00 N/min to failure at room temperature. The specific tensile strength, specific Young's modulus and strain at failure were determined from the stress and strain data signals through dividing values by density of the sample. A one-way analysis of variance (ANOVA) and post hoc Duncan's test was performed for each film to assess the significance of the differences among mechanical properties of the films. The attenuated total reflection–Fourier transform infrared (ATR FT-IR) spectra of neat LCNF, neat CNF, and the composite films were obtained using a Perkin Elmer Spectrum Two ATR-FTIR spectrometer (Waltham, MA). Each sample was scanned from 400 to 4000 cm^{-1}.

An Amray 1820 Scanning Electron Microscope (Amray, Inc./KLA-Tencor Corp., Bedford, MA.) at 10.0 kV was used to analyze the morphology of the films' surface in contact with the dish (dish-side surface) and the surface in contact with air (air-side surface) during the casting process, as well as the structure of their cross-sections after failure.

Results and discussion

LCNF characterization

Because LCNF and CNF suspensions contain both micro and nano scale fibrils, a better strategy to evaluate their particle size and particle size distribution is to combine a micro-scale and nano-scale assessment procedure. In this study, the structures of CNF and LCNFs were determined using light microscopy and AFM. Figure 1 shows the AFM (top) and light microscopy (bottom) images that compare the structure of the reference CNF and LCNFs isolated from the never-dried TMP (LCNF M2) and air-dried TMP (LCNF M3). At a microscale level with light microscopy images, CNF showed a structure forming a random network of defibrillated fibrils (Fig. 1d). A similar structure was observed for LCMF M3 (Fig. 1f) that was less homogeneous in terms of shapes and size, and showed apparent wider fibrils as well as persistent fiber bundles. LCNF M2 (Fig. 1e) however, showed a bulk networked structure with fibrils having an apparent shorter length. The fibril structures observed

at a micro-scale level were in conformity with the nanoscale particle structure observed via AFM (Fig. 1a–c). The softer fibers in the never-dried TMP were easily dispersed in water (at 3% consistency). Milling soft and individualized TMP fibers facilitated the grinding process (100% fine content) and contributed to a shorter processing time. On the other hand, the significant reduction of the water content during the air-drying process led to particle agglomeration and the formation of coarse and stuck chunks, hardly dispersible in water by simple mechanical stirring. Consequently, longer grinding time (3 h) was needed for the air-dried fibers leading to the presence of 80% fines in the slurry, characterizing a reduced efficiency in the process. The coarser and agglomerated fibers used in the process however, did not induce clogging as generally observed for larger particles when using microfuidization (Carrillo Lugo 2014) and high-pressure homogenization (Naderi et al. 2015).

In this work the average fibril diameter and the diameter distribution of CNF and LCNFs were obtained by analyzing images observed by light microscopy (micro-scale level) and AFM (nano-scale level) through an analysis of about 100 measurements. Figure 2 shows the distribution of the nanofiber diameters obtained from the processing of AFM (left) and light microscopy (right) images of CNF (Fig. 2a, b), LCNF M2 (Fig. 2c, d) and LCNF M3 (Fig. 2e, f).

It was observed in all materials that the diameter distribution of the larger fibrils ranged from 1 to 10 μm at a micro-scale level while at a nan-oscale level, AFM images displayed diameters varying between <10 and 1100 nm. The distribution however, varied depending on the type of nanofibrils observed. The reference CNF showed a wide distribution but had higher amount of particles with diameter between 1 and 2 μm as compared to LCNF M2 and M3. However, most of the fibrils in CNF displayed diameters varying between 2 and 3 μm, and 200 and 500 nm (with a peak situated in the range of 200–300 nm) at a microscopic and nanoscopic scales, respectively. A narrower distribution was observed for LCNF M2 both from light microscopy and AFM image processing. The majority of the LCNF M2's fibrils had diameters in the range of 2–4 μm and 100 to 300 nm at a micro-scale and nanoscale, respectively. For LCNF M3 however, a larger distribution was noticed in particle diameter where the number of fibrils with diameter varying between 2 and 6 μm and 200 and 500 nm was higher.
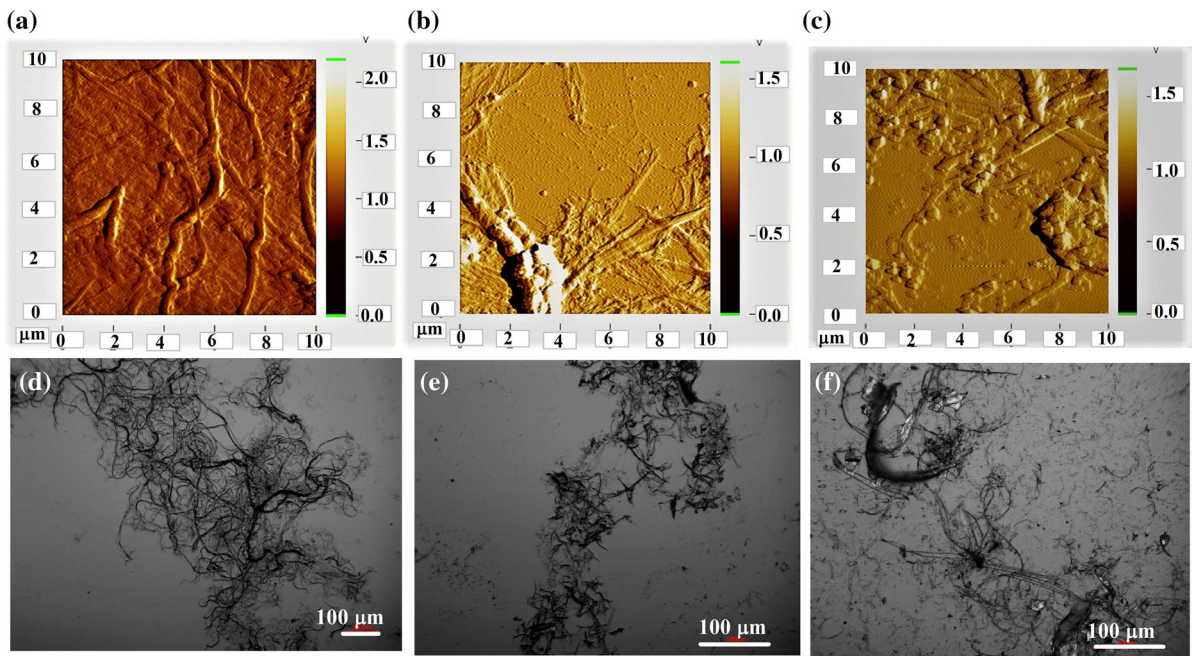
Fig. 1 AFM (*top*) and light microscopy (*bottom*) images that compare the structure of the reference CNF and LCNFs isolated from the never-dried TMP (LCNF M2) and air-dried TMP (LCNF M3)

Overall, the average diameters for the nanofibrils in the different materials at a nanoscale level were 316 ± 99, 239 ± 197 and 425 ± 182 nm for the reference CNF, LCNF M2 and LCNF M3, respectively. When considering the microscopic scale, we obtained average fibril diameters of 2.7 ± 1.6, 2.3 ± 0.7 and 4.3 ± 1.6 μm for CNF, LCNF M2 and LCNF M3, respectively.

LCNFs generally are in the form of random filaments with tiny diameters in the order of nanometer and several micrometers in length. When using the never-dried TMP, the fiber conditions seemed to be affecting particle diameter, since the average diameter of 186 nm and 2 μm (on nano- and micro-scale, respectively) in LCNF M3 was higher as compared to LCNF M2. In addition, the maximum possible amount of fines (100% fines) was reached in LCNF M2 in a shorter processing time evidencing a more effective fibril length shortening.

In literature however, the average fibril diameter of CNF has been reported to range between 20 and 50 nm (Chirayil et al. 2014). Those studies generally determined these dimensions using a transmission electron microscopy (TEM) observation of the nanoparticles, probably missing the larger fiber fractions. In our study, the measurements methods were carried out to

AFM and light microscopy. Other studies found that fibril individualization in LCNF produced from TMP is difficult to achieve due to the presence of lignin that acts as a gluing agent between cellulose fibrils (Osong 2014). When considering the shape of the nanofibrils, difference in structure appeared between the reference CNF made from bleached pulp and LCNF M2 (Fig. 1). However, in terms of particle dimensions, narrower distributions were displayed by LCNF M2. Considering the diameter and diameter distribution as well as fine content in the slurry, LCNF M2 showed better structure as compared to LCNF M3 and therefore was selected for the following steps of our study.

TGA was used to determine the temperature of thermal degradation of the different cellulosic materials. Figure 3 shows the variation of the weight loss and the derivative weight loss (DWL) of TMP, LCNF M2, CNF and lignin (Indulin) as a function of temperature (Fig. 3a, b).

In Fig. 3a, it was observed that the reference CNF showed a better stability at higher temperature compared to LCNF M2 containing lignin and the original TMP. Weight loss curves and DWL showed typical trends of lignocellulosic materials, generally characterized by variations occurring at around 100 °C attributed to water evaporation and between 200 and
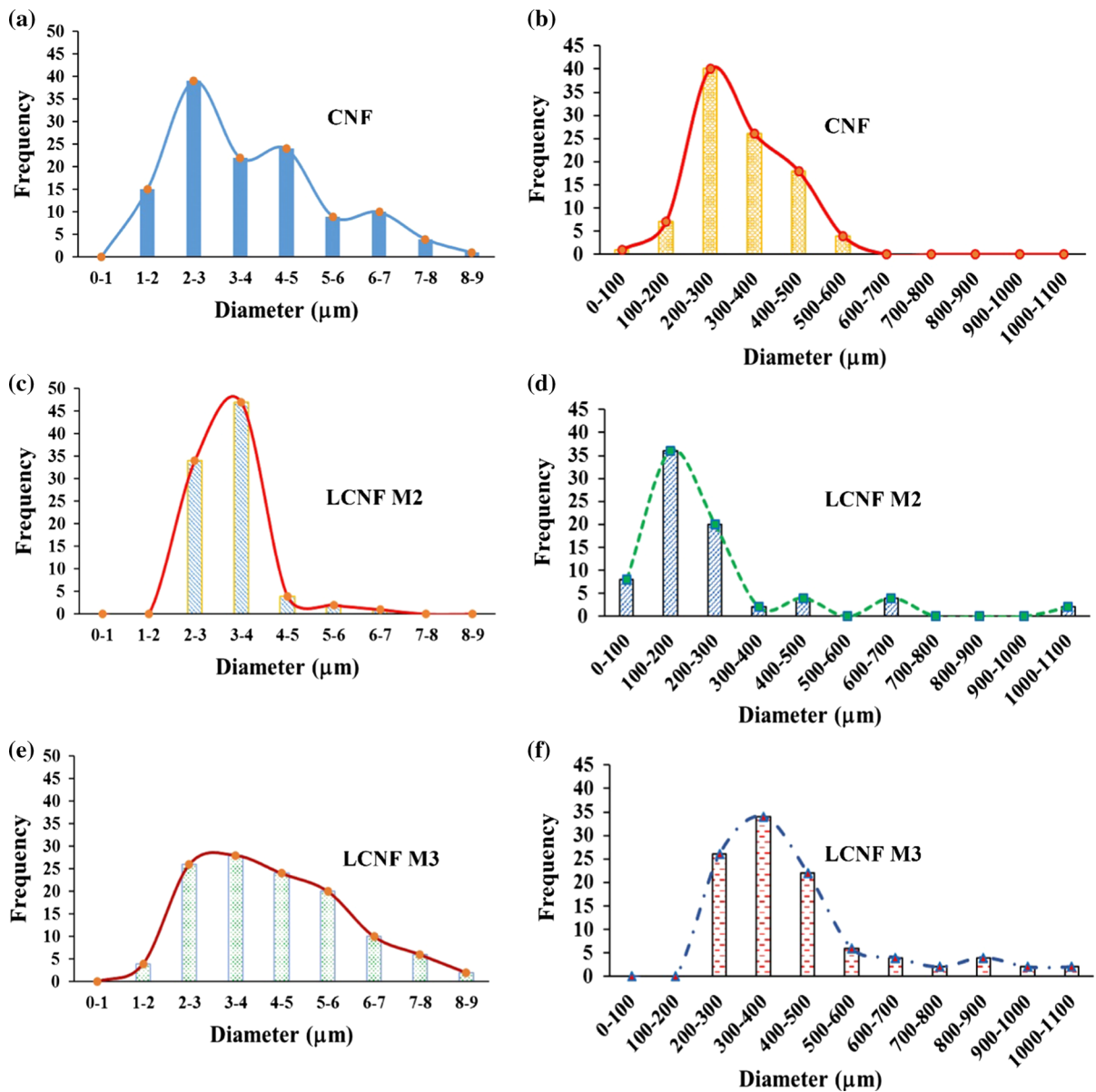
Fig. 2 Distribution of the nanofiber diameters as observed from processing AFM (*left*) and light microscopy (*right*) images of the reference CNF (**a**, **b**), LCNF M2 (**c**, **d**) and LCNF M3 (**e**, **f**)

400 °C that are mostly attributed to the decomposition of hemicellulose and cellulose (Yang et al. 2007), respectively. Similar to TMP, LCNF M2 started to degrade at around 240 °C, while the onset temperature was located at around 270 °C for the reference CNF. This latter was 30 °C higher as compared to TMP and the derived LCNF that have a similar chemical composition. Results obtained from the pyrolysis of lignin showed that the molecule started to degrade at a

very low temperature located at around 150 °C with a very little mass loss rate (lower than 0.25 wt%/°C). Lignin is a natural component of wood and generally represent between 26 and 32% of the most softwood materials (Sjöström 1993). Its presence in the unbleached TMP and the LCNF M2 reduced the stability of the material and explain their lower degradation temperature compared to CNF. On the other hand, maximum degradation occurred at
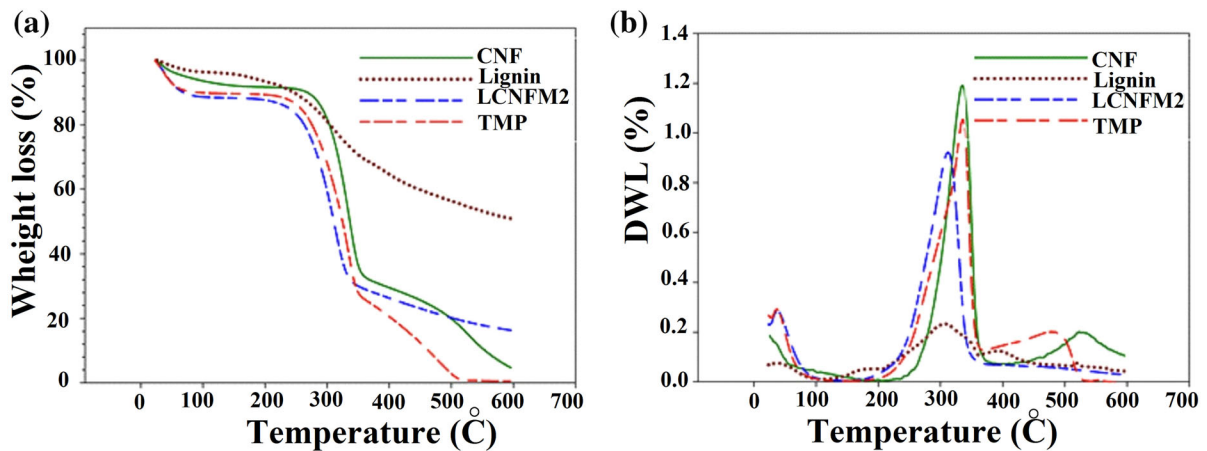
Fig. 3 Weight loss (**a**) and derivative weight loss (**b**) of neat CNF, TMP, LCNF M2 and lignin

temperatures of about 297, 325 and 335 °C for CNF, LCNF M2, and TMP, respectively. These values are in concordance with those found in the literature by authors such as Xiao et al. (2001), Brebu et al. 2013 and Dufresne (2013). The latter found that the temperature for maximum degradation of CNF ranged between 330 and 360 °C depending on the bleaching method. Figure 3a, b show that lignin degraded more slowly and over a large temperature range that starts at around 150 °C and ending near 600 °C. A consistent peak of accelerating weight loss at around 300 °C appeared for the pure lignin and a second peak between 500 and 600 °C was observed for TMP and LCNF M2 that can also be attributed to lignin (Diop et al. 2015).

Table 1 summarizes the onset temperature and maximum temperature of degradation as well as temperature at 10% mass loss of TMP, of the two types of LCNFs, reference CNF, and indulin lignin determined by TGA at a ramp rate of 10 °C/min. It is also observed from Table 1 that LCNF M3 produced

from the air-dried TMP (3 h milling) degraded at temperatures that did not consistently relate to those of LCNF M2. However, 10 and 50% of the LCNF M3 mass were lost at temperatures respectively 10 and 20 °C higher in comparison to LCNF M2.

Figure 4 shows the variation of the weight ratio of the different cellulosic samples as a function of time when undergoing an isothermal heating at 280 °C for
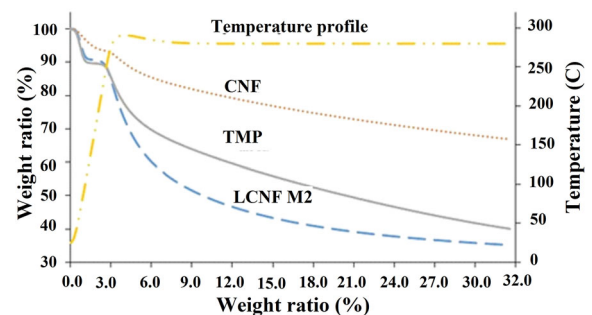

Fig. 4 Isothermal TG curves of CNF, TMP and LCNF M2 as a function of time

Table 1 Thermal stability results of TMP, CNF, LCNFs and lignin (ramp from 25 to 600 °C)

Material	T °C at 10% mass loss (°C)	T °C at 50% mass loss (°C)	Onset temp. of degradation (°C)	Max temp. of degradation (°C)
TMP	274.2 ± 0.5	331.4 ± 0.4	239.8 ± 0.5	335.6 ± 0.5
LCNF M2	265.6 ± 2.6	319.8 ± 4.0	247.9 ± 2.4	325.8 ± 5.2
LCNF M3	273.8 ± 2.2	332.2 ± 3.8	240.3 ± 1.2	337.8 ± 0.3
CNF	293.7 ± 0.8	339.2 ± 0.1	270.8 ± 0.4	297.1 ± 9.6
Lignin*	266.0 ± 0.4	545.0 ± 3.9	128.2 ± 2.0	297.1 ± 9.6

* INDULIN AT Lignin first major peak of degradation between 0 and 600 °C

30 min. When subjected to isothermal TGA, it was observed that the lignin-containing materials degraded faster than CNF. $66.8 \pm 0.7\%$ of the original mass of CNF was left after the pyrolysis period, while the residual masses after 30 min of isothermal test were 40.1 ± 0.2 and $35.2 \pm 1.6\%$ for TMP and LCNF M2, respectively. In the first 10 min of the isothermal pyrolysis at temperature of 280 °C, approximately 38% of the TMP and 50% of the LCNF decomposed whereas only 18% of the CNF had decomposed.

This can be attributed to the fact that lignin and hemicellulose make up approximately 30–65 wt% of unbleached softwood biomass and start degradation well below 280 °C (Yang et al. 2007). After 10 min the rate of weight loss became constant at approximately 6 wt%/min for TMP and LCNF M2 and 4 wt%/min for the CNF. This shows that the decomposition of lignin and hemicellulose accelerated the rate of mass loss once the furnace was held isothermal. Lignin's polymer structure is known to decompose typically through aryl-ether bond cleavage that has high potential to form radicals and increase the rate of degradation (Yang et al. 2007; Xiao et al. 2001).

Mechanical properties of LCNF composite films

The mechanical properties of neat CNF and neat LCNF films (made from LCNF M2), as well as composite films, were determined. Figure 5 shows the specific Young's modulus (Fig. 5a) and specific tensile strength (Fig. 5b) of different films. The composite films were made of LCNF matrix reinforced with 10 wt% additive.

The specific Young's modulus and the specific tensile strength of the neat CNF films with values of 35.5 ± 4 GPa g^{-1} cm^3 and 80.7 ± 5 MPa g^{-1} cm^3 were respectively 7.6 GPa g^{-1} cm^3 and 46.8 MPa g^{-1} cm^3 higher as compared to the neat LCNF films. A film made of TEMPO-oxidized CNF reported by Qing et al. (2012) showed a higher tensile strength value of 232 MPa. However, its Young's modulus value (4.79 GPa) was significantly lower as compared with the neat CNF film discussed in this work. The samples tested by Qing et al. (2012) also had much higher densities around 1.4 g/cm^3. The presence of lignin in LCNF could explain both the reduction of the film stiffness and increased film plasticity. However, Spence et al. (2010) found that the presence of lignin significantly increased the toughness, tensile index and elastic modulus of films made from a combined refined and high-pressure homogenized microfibrillated cellulose. On the other hand, CNF films showed higher density than LCNF with respective values of 1.07 and 0.81 g/cm^3. These values were high compared to hot-pressed films where lignin softening could induce filling of voids within the films (Spence et al. 2010). The difference in the film production methods and the variation of lignin contents in other studies does not allow for direct comparison between the densities and mechanical properties seen in this paper (Osong 2014; Rojo et al. 2015).

However, general trends agree such that LCNF films are less dense and had inferior mechanical properties than those of CNF. The neat CNF film was much stronger and more ductile than the neat LCNF film as seen in Fig. 5.
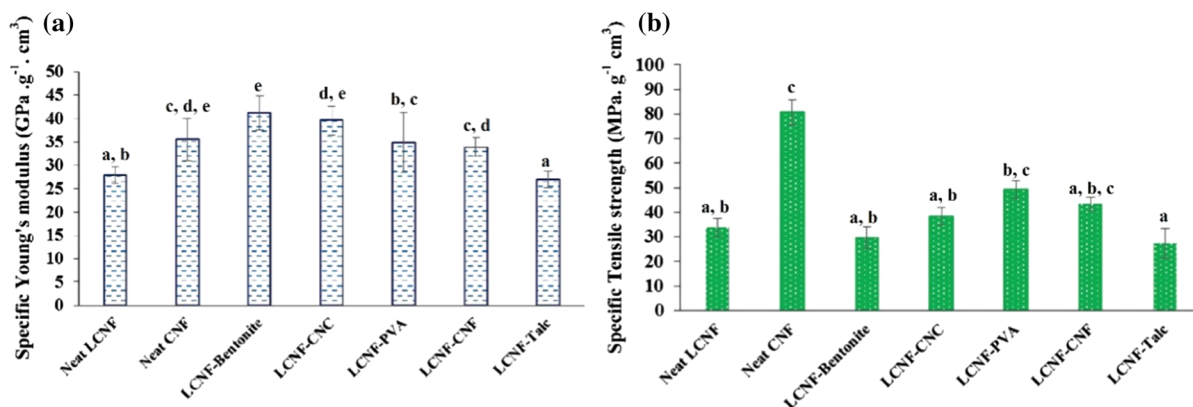

Fig. 5 Variation of the specific Young's modulus and specific tensile strength of the neat CNF, the neat LCNF and the LCNF composite films

The addition of additives in the LCNF composite films was shown to increase the mechanical properties as observed in Fig. 5a, b. Adding bentonite and CNC improved the specific Young's modulus of the LCNF films to values surpassing that of the neat CNF films. On the other hand, the LCNF/PVA film showed similar elastic modulus to that of neat CNF films, whereas a reduction of the modulus values previously observed for the neat CNF was not obtained by the incorporation of CNF in the LCNF film. In terms of tensile strength, concrete improvement was obtained by adding CNC, CNF and particularly PVA in the LCNF matrix, however, the strengths of these films were significantly lower as compared to that observed for the neat CNF film.

Tables 2 and 3 show respectively the significance of the differences in tensile strength and Young's modulus values of the neat and composite films obtained from Duncan's multiple range tests. The statistical test revealed that the specific strengths of the neat LCNF and the composite films containing, CNF and PVA were not significantly different at 95% significance level. In addition, none of the additives were able to significantly improve specific tensile strength of LCNF films.

Interestingly, replacement of 10% of the LCNF film with CNF significantly improved specific Young's modulus of the film to a level that it did not show a significant difference with CNF. This is an important finding as it shows despite the original inferior stiffness of CNF, it is possible to improve this property by adding 10% CNF to the formulation. CNC and bentonite also caused a similar improvements leading to specific Young's modulus values exceeding that of neat CNF. Overall, the mechanical properties of the neat CNF films was significantly higher as compared to the neat LCNF films. The difference in chemical composition, mostly the presence of lignin between these two nanofibril-based films as well as differences in particle size and particle size distribution could explain this difference.

Table 4 summarizes the density and the strain at failure values of neat LCNF and LCNF composite

Table 2 Homogeneous subsets Duncan's tests for specific tensile strength of the neat and composite films

Formulation	N	Subset for alpha = 0.05		
		1 (a*)	2 (b*)	3 (c*)
LCNF/talc	5	25.1		
LCNF/bentonite	4	26.4	26.4	
Neat LCNF	5	34.1	34.1	
LCNF/CNC	5	36.4	36.4	
LCNF/CNF	5	43.6	43.6	43.6
LCNF/PVA	5		47.0	47.0
Neat CNF	5			61.9
Significance		0.088	0.057	0.074

* Common lowercase letters denote non-significant differences at 95% confidence level

Table 4 Density and strain at failure results of the neat and LCNF composite films

Material	Density (g/cm^3)	Strain at failure (%)
Neat CNF	1.07 ± 0.05	7.7 ± 1.3
Neat LCNF	0.81 ± 0.02	1.9 ± 0.4
LCNF/TALC	0.81 ± 0.05	1.7 ± 0.6
LCNF/bentonite	0.94 ± 0.02	0.98 ± 0.14
LCNF/CNC	0.82 ± 0.02	1.5 ± 0.3
LCNF/PVA	0.73 ± 0.01	2.2 ± 0.3
LCNF/CNF	0.90 ± 0.02	2.6 ± 0.4

Table 3 Homogeneous subsets Duncan's tests for the specific Young's modulus of the neat and composite films

Formulation	N	Subset for alpha = 0.05				
		1 (a*)	2 (b*)	3 (c*)	4 (d*)	5 (e*)
LCNF/Talc	5	26.7				
Neat LCNF	5	28.0	28.0			
LCNF/PVA	5		32.6	32.6		
LCNF/CNF	5			34.0	34.0	
Neat CNF	4			37.3	37.3	37.3
LCNF/CNC	5				38.8	38.8
LCNF/Bentonite	4					40.0
Significance		0.608		0.078	0.092	0.083	0.316

* Common lowercase letters denote non-significant differences at 95% confidence level

films. Adding bentonite decreased the ductility of
LCNF films from $1.9 \pm 0.4\%$ strain at failure to
$0.98 \pm 0.14\%$ strain at failure. Talc has been reported
to induce flexible films with good mechanical prop-
erties, when incorporated in CNC films (Liimatainen
et al. 2013). In our study, the addition of talc to the
LCNF did not bring about any additional mechanical
performance film. The fact that commercial talc
generally tends to aggregate in aqueous media as
observed by Liimatainen et al. (2013) causing an
inhomogeneous distribution throughout the film could
be responsible of the low mechanical properties and its
low reinforcing ability for composite materials.

The low density and superior mechanical properties
of the LCNF/PVA films gives an alternative to CNF
depending on the process conditions and application.
PVA is a biodegradable additive and there is no
chemical waste associated with producing LCNF from
unbleached TMP. Micro-grinding is also a more
energy efficient production method of producing
LCNF than homogenization or micro-fluidization so
there are many factors to consider when choosing the
nanofibril material for films (Spence et al. 2011).

Physico-chemical properties of composite films

Figure 6 shows the FT-IR spectra of the neat LCNF
(made from LCNF M2) and CNF films (Fig. 6a) as
well as the different LCNF composite films (Fig. 6b).
As compared to the neat CNF film, the LCNF film's
spectrum was characterized by a reduction of the
intensities of the two peaks appearing at around
3330 cm^{-1} and 2903 cm^{-1}. These peaks are generally
attributed to the aromatic and aliphatic O–H stretching
intramolecular hydrogen bonds for cellulose and to the
C-H stretching vibrations of methyl (CH_2), respec-
tively (Diop et al. 2015). This reduction could confirm
the lower presence of free OH groups in LCNF as
compared to its bleached counterpart. It was observed
that the peaks generally attributed to the C–O–C
pyranose ring stretching vibration and to the cellulosic
glycosidic linkages (1028 cm^{-1}), to the CH_2 scissor-
ing motion in cellulose (1430 cm^{-1}) and to the CH_2
rocking vibration at C6 carbon (1314 cm^{-1}) were
visible in the LCNF spectrum. The acetyl and uronic
ester groups of hemicellulose or the ester linkage of
carboxylic group of ferulic and p-coumaric acids of
lignin and/or hemicelluloses were characterized by the
peaks at around 1740 cm^{-1}.

Other peaks appearing at 1599 and 1515 cm^{-1}
could be related to the C=C vibration of the aromatic
ring in the residual lignin and the peak at 1263 cm^{-1}
could be assigned to the O–H deformation arising
from phenolic group (C–OH stretching), respectively
(Diop et al. 2015). These characteristic peaks
attributed to lignin and hemicellulose were still
observed in different composite films where they
appeared with a lower intensity. For the LCNF/PVA
composite films, some characteristics peaks at around
1713 and 1420 cm^{-1} attributed to carbonyl functional
group of the residual acetate group remaining after the
manufacture of PVA and to the CH_2 bond in the neat
PVA film did not appear in the composite film. The
same observations were obtained for composite films
containing bentonite and talc. Some characteristic
infrared bands of bentonite generally attributed to Si–
O stretching (1048 cm^{-1}), Al–OH–Al bending
(918 cm^{-1}), Al–OH–Fe bending (876 cm^{-1}) and
Al–OH–Mg bending (843 cm^{-1}) (Madejova and
Komadel 2001) were not clearly observed in the
LCNF/bentonite composite films. Similarly, for pure
talc, the sharp OH stretching at 3674 cm^{-1} did not
influence the LCNF/talc film spectra. Other peaks at
667, 1004 and 3562 cm^{-1}, commonly attributed to the
symmetric Si–O–Si stretching, the asymmetric Si–O–
Si stretching and the brucite layer hydroxyl group of
chlorite in talc (Belgacem et al. 2008) were not
remarkably observed.

The water absorption (WA%) of neat LCNF, neat
CNF, and different composite films was analyzed
during a period of 180 min. Neat PVA films were also
tested for comparison. Figure 7 shows the evolution of
the water absorption of the neat and composite films.
Most of the weight gain of the films due to water
absorption occurred during the first 30 min of soaking.
LCNF films showed a lower water absorption as
compared to neat CNF film references. Neat PVA
films showed the highest water absorption values.
With the increase of the soaking time from 30 to
180 min, WA% increased slightly in all tested films.

The presence of lignin in LCNF that has higher
hydrophobicity as compared to the neat CNF could
explain the lower WA% noticed for the neat LCNF
film. PVA, in contrast is a highly hydrophilic material
because of the hydroxyl groups that enable hydrogen
bonding to be formed with water (Li et al. 2012; Yee
et al. 2011). As expected, the incorporation of PVA in
the LCNF matrix contributed to an increase of the

Fig. 6 Comparison of the FT-IR spectra between CNF and LCNF films (**a**) and FT-IR spectra of the LCNF composite films (**b**)
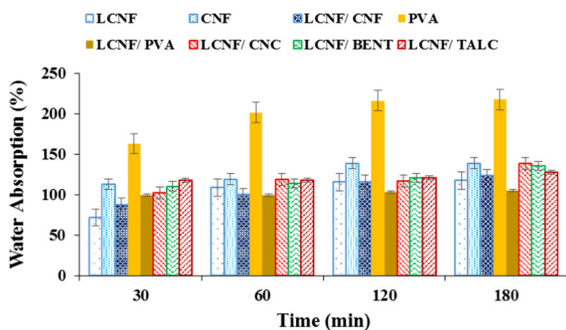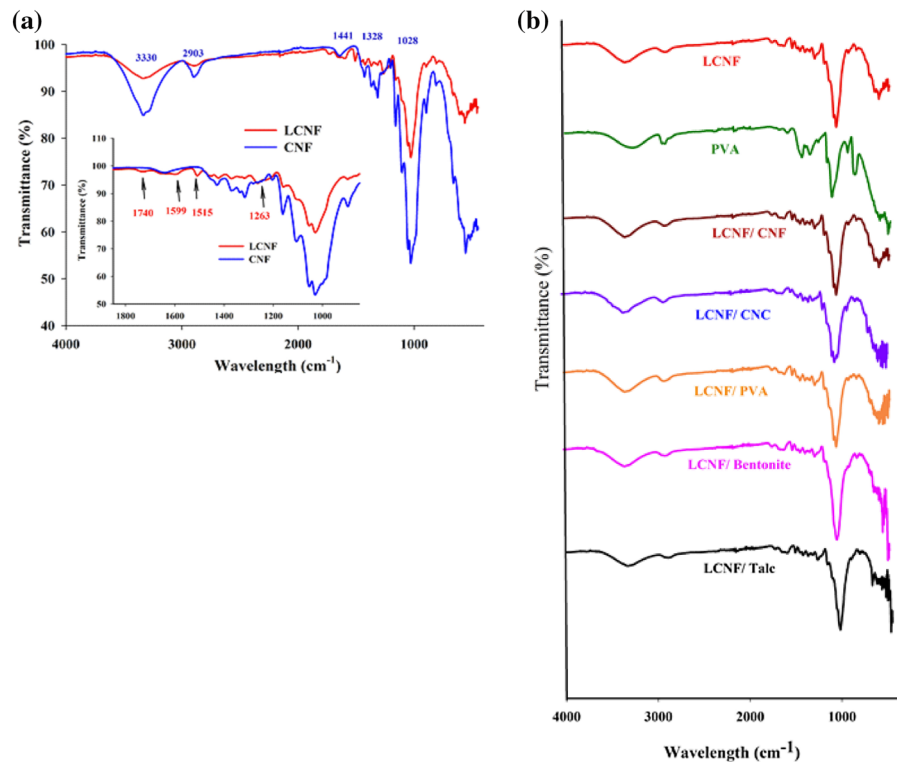

Fig. 7 Evolution of the water absorption of neat CNF, neat LCNF and LCNF composite films during 180 min soaking

WA% observed in the LCNF film, however, the water absorption of the LCNF/PVA films did not show any changes after the initial 30 min of soaking period. Overall, lower WA% was obtained for neat LCNF films, and the addition of additives resulted in higher water absorption. LCNF-CNC, LCNF/Bentonite, and LCNF/talc started to disintegrate after 60 min of soaking. Qing et al. (2012) attributed the film dissociation observed at high water content to dissociation of the hydrogen bonds between nanofibers. Inversely, the dry strength of the neat LCNF, CNF, and PVA films as well as LCNF/PVA and LCNF/CNF

composite films was not strongly affected. Nair and Yan (2015) stated that that high-lignin nanofibril films retained 38% of the dry strength properties, while the low-lignin nanofibril films were able to retain only 9% of dry strength.

Scanning electron microscopy was used to evaluate the film surfaces and cross-sections. Figure 8 shows the SEM images of the side of an LCNF/PVA film exposed to the air (Fig. 8a) and the surface in contact of the petri dish (dish side) (Fig. 8b) while being cast. There was a considerable difference in the roughness associated with the two side of the films. Rojo et al. 2015 found that the roughness of LCNF nanopapers decreased with the increasing lignin content. As can be seen, few voids were likely formed on the dish side of the film from trapped air bubbles.

Figure 9, which shows the SEM image of the fractured cross section of the neat LCNF, neat CNF, as well as LCNF/CNF and LCNF/CNC composite films that clearly depict the lamellar structure and voids throughout the film. This lamellar structure appearing on the cross section was also reported by Qing et al. (2012) for neat CNF and CNF/phenol formaldehyde composite films. This is believed to be due to the fact that the fibrils tend to form clusters of layered sheets
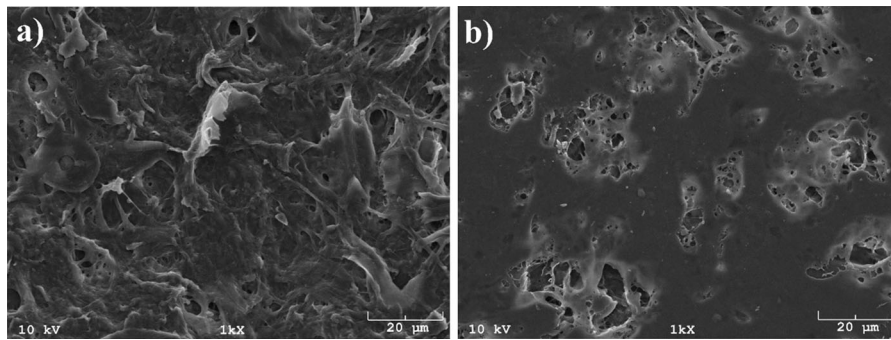
Fig. 8 SEM images of the air dried side (**a**) and side in contact to the dish of (**b**) LCNF-PVA film after a casting evaporation method
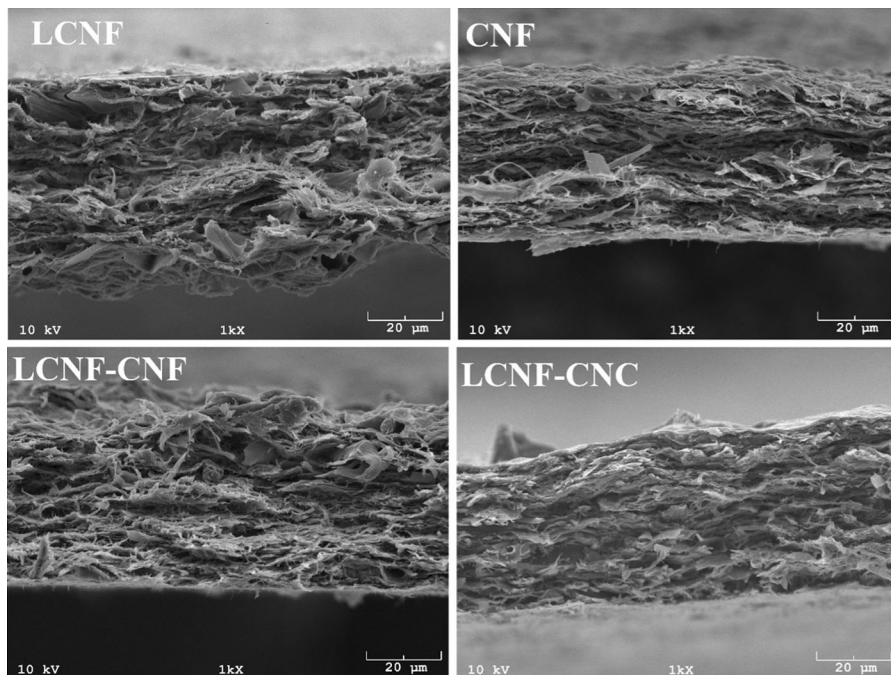

Fig. 9 Images of the fractured cross section of the neat LCNF, neat CNF as well as LCNF/CNF and LCNF/CNC composite films

leaving voids. This finding agrees with other studies where the nanofibrils were found to be organized in layers with their principal axis in the plane of the film (Rojo et al. 2015).

Compared to the LCNF films, where larger voids were observed, a denser interface layer was observed for the neat CNF films. Blending these two types of nanofibrils did not consistently densify the LCNF film layer, nor reduced the void size. On the other hand, a better compaction was observed from the structure of the LCNF/CNC cross-section. Other reports on nanopapers containing residual lignin have found that film thickness decreases with increased lignin content

(Ferrer et al. 2012). Their tested nanopapers however, underwent a hot-pressing at high temperature and pressure that compacted the sheet and softened the lignin. This latter acted as a natural binder resin in the pressed films, decreasing apparent voids number, which in turn decreased the film roughness and thickness.

Conclusions

The present work investigated the effect of the type of TMP (never-dried or air-dried) used for the production

of lignocellulose nanofibrils (LCNF). Using air-dried TMP resulted in longer milling time with lower defibrillation and lower fine content in the slurry as compared to never-dried TMP. The initial water content clearly affected the structure, shape and dimensions of the LCNFs. The average fibril diameter distribution measured at a nanoscopic level using AFM images was in the range of 316 ± 99, 239 ± 197 and 425 ± 182 nm for the reference CNF, LCNF M2 and LCNF M3, respectively. When considering the microscopic scale, we obtained average fibril diameters of 2.7 ± 1.6, 2.3 ± 0.7 and 4.3 ± 1.6 μm for CNF, LCNF M2 and LCNF M3, respectively.

The onset temperatures of degradation for TMP as well as LCNF were around 30 °C lower when compared to the onset temperature of the reference CNF isolated from bleached pulp. This reduction was attributed to the presence of lignin. LCNF M2 having higher fine percent and a narrower fibril diameter distribution was chosen as the matrix for the production of composite films. Different additives were used to reinforce the film matrix. Neat films produced from lignocellulosic nanofibrils were slightly less dense than films made from bleached CNF but had significantly lower mechanical properties. It was shown in this study however, that with the addition of other materials to the LCNF film matrix, more desirable mechanical properties could be obtained. For instance, adding PVA to LCNF film increased the Young's modulus of the LCNF film to the extent to surpass the stiffness of films made of CNF. CNF is much more ductile and stronger than LCNF and the addition of other additives did not allow an improvement of film properties to a magnitude similar to that of the CNF film. On the other hand, due to the presence of a more hydrophobic lignin, LCNF showed a lower water absorption that increased with its reinforcement with additives. SEM images showed layered cross sections with appearing voids after casting. It is important to note that LCNF has the potential to be used as an alternative to CNF, but there are trade-offs associated with making this change. LCNF is much simpler and more energy efficient to produce without any chemical wastes, but there is less thermal stability and films will be weaker and may require additives to achieve the desired mechanical properties.

References

Belgacem K, Llewellyn P, NNahdi K, Trabelsi-Ayadi M (2008) Thermal behaviour study of the talc. Optoelectron Adv Mat Rapid Comm 2:332–336

Bharimalla AK, Deshmukh SP, Patil PG, Vigneshwaran N (2015) Energy efficient manufacturing of nanocellulose by chemo- and bio-mechanical processes: a review. World J Nano Sci Eng 5:204–212. doi:10.4236/wjnse.2015.54021

Brebu M, Tamminen T, Spiridon I (2013) Thermal degradation of various lignins by TG-MS/FTIR and Py-GC-MS. J Anal Appl Pyrol 104:531–539

Carrillo Lugo CA (2014) Application of complex fluids in lignocellulose processing. Dissertation, North Carolina State University, 178 p

Chirayil CJ, Mathew L, Thomas S (2014) Review of recent research in nano cellulose preparation from different lignocellulosic fibers. Rev Adv Mater Sci 37:20–28

Diop CIK, Lavoie JM, Huneault MA (2015) Structural changes of Salix miyabeana cellulose fibres during dilute-acid steam explosion: impact of reaction temperature and retention time. Carbohyd Polym 119:8–17

Dufresne A (ed) (2013) Thermal degradation of cellulose. In: Nanocellulose: from nature to high performance tailored materials, chap 8.4.1. Walter de Gruyter GmbH, Berlin, p 283

Ferrer A, Filpponen I, Rodríguez A, Laine J, Rojas OJ (2012) Valorization of residual Empty Palm Fruit Bunch Fibers (EPFBF) by microfluidization: production of nanofibrillated cellulose and EPFBF nanopaper. Bioresour Technol 125:249–255

Khalil HA, Davoudpour Y, Islam MN, Mustapha A, Sudesh K, Dungani R, Jawaid M (2014) Production and modification of nanofibrillated cellulose using various mechanical processes: a review. Carbohyd Polym 99:649–665

Kojima Y, Isa A, Kobori H, Suzuki S, Ito H, Makise R, Okamoto M (2014) Evaluation of binding effects in wood flour board containing ligno-cellulose nanofibers. Materials 7(9):6853–6864

Li W, Yue J, Liu S (2012) Preparation of nanocrystalline cellulose via ultrasound and its reinforcement capability for poly (vinyl alcohol) composites. Ultrason Sonochem 19(3):479–485

Liimatainen H, Ezekiel N, Sliz R, Ohenoja K, Sirviö JA, Berglund L, Hormi O, Niinimäki J (2013) High-strength nanocellulose–talc hybrid barrier films. ACS Appl Mater Interfaces 5(24):13412–13418

Madejova J, Komadel P (2001) Baseline studies of the clay minerals society source clays: infrared methods. Clay Clay Miner 49:410–432

Naderi A, Lindström T, Sundström J (2015) Repeated homogenization, a route for decreasing the energy consumption in the manufacturing process of carboxymethylated nanofibrillated cellulose. Cellulose 22(2):1147–1157

Nair SS, Yan N (2015) Effect of high residual lignin on the thermal stability of nanofibrils and its enhanced mechanical performance in aqueous environments. Cellulose 22(5):3137–3150

Osong SH (2014). Mechanical pulp based nano-ligno-cellulose: production, characterisation and their effect on paper properties. Thesis of the degree of Licentiate of Technology, Mid Sweden University, p 57

Osong SH, Norgren S, Engstrand P (2013) An approach to produce nano-ligno-cellulose from mechanical pulp fine materials. Nord Pulp Pap Res J 28(4):472–479

Qing Y, Sabo R, Wu Y, Cai Z (2012) High-performance cellulose nanofibril composite films. BioResources 7(3):3064–3075

Rojo E, Peresin MS, Sampson WW, Hoeger IC, Vartiainen J, Laine J, Rojas OJ (2015) Comprehensive elucidation of the effect of residual lignin on the physical, barrier, mechanical and surface properties of nanocellulose films. Green Chem 17(3):1853–1866

Sjöström E (1993) Wood chemistry: fundamentals and applications. Academic, New York

Spence KL, Venditti RA, Rojas OJ, Habibi Y, Pawlak JJ (2010) The effect of chemical composition on microfibrillar cellulose films from wood pulps: water interactions and physical properties for packaging applications. Cellulose 17(4):835–848

Spence KL, Venditti RA, Rojas OJ, Habibi Y, Pawlak JJ (2011) A comparative study of energy consumption and physical properties of microfibrillated cellulose produced by different processing methods. Cellulose 18(4):1097–1111

Wear D, Prestemon J, Foster MO (2015) US forest products in the global economy. J For 114(4):483–493

Xiao B, Sun X, Sun R (2001) Chemical, structural, and thermal characterizations of alkali-soluble lignins and hemicelluloses, and cellulose from maize stems, rye straw, and rice straw. Polym Degrad Stabil 74(2):307–319

Yang H, Yan R, Chen H, Lee DH, Zheng C (2007) Characteristics of hemicellulose, cellulose and lignin pyrolysis. Fuel 86(12):1781–1788

Yee TW, Choy LJ, Rahman WAWA (2011) Mechanical and water absorption properties of poly (vinyl alcohol)/sago pith waste biocomposites. J Compos Mater 45(11):1201–1207